MBoC | ARTICLE

Bacterial growth dynamics in a rhythmic symbiosis

Liu Yang[a,b], Susannah Lawhorn[b], Clotilde Bongrand[b], James C. Kosmopoulos[c,d], Jill Kuwabara[a,b], Michael VanNieuwenhze[e], Mark J. Mandel[c,d,f], Margaret McFall-Ngai[a,b,g], and Edward Ruby[a,b,g,*]

[a]Carnegie Institution for Science, Pasadena, CA 91101; [b]Pacific Biosciences Research Center, University of Hawaii at Manoa, Honolulu, HI 96848; [c]Department of Bacteriology, [d]Microbiology Doctoral Training Program, and [f]Department of Medical Microbiology & Immunology, University of Wisconsin-Madison, Madison, WI 53706; [e]Department of Chemistry, Indiana University Bloomington, Bloomington, IN 47405; [g]Division of Biology & Biological Engineering, California Institute of Technology, Pasadena, CA 91125

ABSTRACT **The symbiotic relationship between the bioluminescent bacterium *Vibrio fischeri* and the bobtail squid *Euprymna scolopes* serves as a valuable system to investigate bacterial growth and peptidoglycan (PG) synthesis within animal tissues. To better understand the growth dynamics of *V. fischeri* in the crypts of the light-emitting organ of its juvenile host, we showed that, after the daily dawn-triggered expulsion of most of the population, the remaining symbionts rapidly proliferate for ~6 h. At that point the population enters a period of extremely slow growth that continues throughout the night until the next dawn. Further, we found that PG synthesis by the symbionts decreases as they enter the slow-growing stage. Surprisingly, in contrast to the most mature crypts (i.e., Crypt 1) of juvenile animals, most of the symbiont cells in the least mature crypts (i.e., Crypt 3) were not expelled and, instead, remained in the slow-growing state throughout the day, with almost no cell division. Consistent with this observation, the expression of the gene encoding the PG-remodeling enzyme, L,D-transpeptidase (LdtA), was greatest during the slowly growing stage of Crypt 1 but, in contrast, remained continuously high in Crypt 3. Finally, deletion of the *ldtA* gene resulted in a symbiont that grew and survived normally in culture, but was increasingly defective in competing against its parent strain in the crypts. This result suggests that remodeling of the PG to generate additional 3–3 linkages contributes to the bacterium's fitness in the symbiosis, possibly in response to stresses encountered during the very slow-growing stage.**

SIGNIFICANCE STATEMENT

- We focus on patterns of a specific bacterial symbiont's peptidoglycan (PG)-synthesis activity, a critical process supporting bacterial growth and survival from the perspectives of both developmental time (i.e., over different stages of tissue colonization) and spatial locations (i.e., between different tissue-colonization sites).
- The discovery that PG-synthesis activity varies across different stages and locations during a beneficial infection provides insights into how both mutualistic and pathogenic bacteria must adapt to, and survive long-term within, the diverse host tissue conditions.
- This knowledge will improve our grasp of bacterial persistence strategies and their roles in animal-microbe interactions.

Monitoring Editor
Erin Goley
Johns Hopkins University

Received: Feb 1, 2024
Revised: Apr 1, 2024
Accepted: Apr 4, 2024

New Hypothesis

This article was published online ahead of print in MBoC in Press (http://www.molbiolcell.org/cgi/doi/10.1091/mbc.E24-01-0044) on April 10, 2024.

Competing interests: The authors declare no competing interests.

Author Contributions: Conceptualization: L.Y. and E.R.; Methodology: L.Y., M.M.-N. and E.R.; Investigation: L.Y., S.L., C.B., J.T.K., M.J.M., and J.C.K.; Resources: M.M.-N. and E.R.; Provision of fluorescent D-amino acids (HADA and EDADA): M.S.V.; Writing: L.Y. and E.R.; Funding acquisition: E.R., M.M.-N. and M.J.M.

*Address correspondence to: Edward Ruby (eruby@caltech.edu)

Abbreviations used: CFU, colony-forming units; D-Ala, D-alanine; D-Glu, D-glutamate; DMSO, dimethyl sulfoxide; EDADA, alkyne-D-alanine-D-alanine; FSOW, filter-sterilized ocean water; GFP, green fluorescent protein; GlcNAc, *N*-acetyl glucosamine; GTase, glycosyl transferase; HADA, HCC-amino-D-alanine; HCR, hybridization chain-reaction fluorescence in situ hybridization; hpd, hours past dawn; L-Ala, L-alanine; LBS, Luria broth plus salt; LDT, L-D transpeptidase; meso-DAP, meso-diaminopimieic acid; MFA, marker frequency analysis; mPBS, marine phosphate-buffered saline; MurNAc, *N*-acetyl muramic acid; OD, optical density (600 nm); PBP, penicillin-binding protein; PFA, paraformaldehyde; PG, peptidoglycan; PGRP, peptidoglycan receptor protein; RCI, relative colonization index; RFP, red fluorescent protein; SD, standard deviation; TCT, tracheal cytotoxin; TPase, D,D-transpeptidase.

INTRODUCTION

Vibrio fischeri, a marine luminescent bacterium, engages in a species-specific symbiotic relationship with the nocturnally active squid, *Euprymna scolopes*, inhabiting a unique light-emitting organ that aids the squid in a camouflaging behavior known as counterillumination (Nyholm and McFall-Ngai, 2021; Visick *et al.*, 2021). The two halves of this specialized organ each house three separate growth chambers referred to as Crypts 1, 2, and 3 (Figure 1A), which arise embryologically in that order, and range at hatching from the most (Crypt 1) to the least (Crypt 3) developed (Nyholm and McFall-Ngai, 2021). Immediately after the juvenile squid emerges from its egg, symbiont recruitment begins; briefly, *V. fischeri* cells in the surrounding seawater aggregate outside of the organ (Figure 1A), migrate through surface pores into the interior crypts where they proliferate and induce luminescence (Visick *et al.*, 2000; Koch *et al.* 2014; Moriano-Gutierrez *et al.*, 2019). Each morning thereafter, 95% of the total symbiont population is expelled into the surrounding seawater (McFall-Ngai and Ruby, 1991); the remaining symbiont cells proliferate during the day, repopulating the crypts to restore their full bioluminescence capability by dusk (Nyholm and McFall-Ngai, 2021; Visick *et al.*, 2021). Crypts 1 and 2 are larger and more developed than Crypt 3, which has a different tissue environment and venting behavior (Essock-Burns *et al.*, 2020, 2023). For example, the immature Crypt 3 does not begin to exhibit the typical daily cycle of expulsion and regrowth of its symbiont population until 72 h or more after hatching and colonization (Essock-Burns *et al.*, 2020). In addition, recent data have shown that the bacteria in Crypt 3 are better able to withstand environmental disturbance, and can serve as a reservoir for recolonization. Taken together, these and other characteristics suggest that the symbionts in Crypt 3 experience a distinct microenvironment and growth dynamics compared with Crypts 1 and 2 (Dunn *et al.*, 2006; Stoudenmire *et al.*, 2018; Guckes *et al.*, 2019; Essock-Burns *et al.*, 2023).

While bacterial growth, often focusing on the exponential phase, has been extensively studied in culture media, the proliferation of bacteria under more natural environmental conditions, such as within a host's tissues, remains less well understood. This knowledge gap is particularly relevant for bacteria like *V. fischeri* that must undergo a habitat transition between the ambient environment and the host (Bennett *et al.*, 2020; Meyer *et al.*, 2022). Recent studies have collectively underscored the complexity of bacterial growth dynamics within the light organ, highlighting variations in the symbionts' proliferation rates and environmental adaptions that diverge significantly from those observed in standard culture media (Dunn *et al.*, 2006; Stoudenmire *et al.* 2018; Guckes *et al.* 2019). In the light-organ crypts, *V. fischeri* faces biochemical challenges such as antimicrobial peptides, oxidative/nitrosative bursts, acidic pH, and nutritional limitations (Graf *et al.*, 1994; Bosco-Drayon *et al.*, 2012; Mandel *et al.*, 2012). The symbionts also encounter host peptidoglycan-recognition proteins (PGRPs) that act either as degradative amidases or signal transduction receptors responding to the presence of environmental bacteria (Bosco-Drayon *et al.*, 2012). In the squid-vibrio symbiosis, we are just beginning to learn how *V. fischeri* navigates the host's recognition of its peptidoglycan (PG) by these immune receptors (Troll *et al.*, 2009, 2010). Changes in PG structure have been reported in several bacterial pathogens grown under laboratory conditions, and those modifications have been linked to immune evasion; i.e., in the absence of such modifications, pathogenicity is often attenuated (Hernández *et al.*, 2022; Boamah *et al.*, 2023). Much less is known about PG biosynthesis by beneficial bacteria, and how this process might promote a stable symbiosis.

PG synthesis is crucial for bacterial elongation and envelope integrity, forming an interconnected meshwork that surrounds the cell, protecting it from changes in osmotic pressure and other environmental stresses (Typas *et al.*, 2012; Egan *et al.*, 2020). However, our understanding of PG synthesis and remodeling remains limited in beneficial bacteria as they reside long-term within animal tissues. PG structure consists of glycan strands crosslinked by short peptide chains that together form an interconnected meshwork surrounding the cell membrane and providing rigidity to its shape (Typas *et al.*, 2012; Egan *et al.*, 2020). In most bacteria, the sugar backbone is made of alternating *N*-acetylmuramic acid (MurNAc) and *N*-acetylglucosamine (GlcNAc) residues connected by β-1,4-glycosidic linkages (Typas *et al.*, 2012; Egan *et al.*, 2020). Each MurNAc residue is attached to a pentapeptide chain, or stem peptide, which consist of (in order): L-alanine (L-Ala), D-glutamic acid (D-Glu), meso-diaminopimelic acid (meso-DAP), and a di-D-alanine (D-Ala-D-Ala; Vollmer and Bertsche, 2008; Vollmer *et al.*, 2008; Morè *et al.*, 2019). The stem peptide forms three to four crosslinks between glycan strands, in which the amino group at the 3rd position of one peptide acts as an acyl acceptor, and covalently binds the carboxyl group at the 4th position of another peptide (Garde *et al.*, 2021). Synthesis of this meshwork is catalyzed by penicillin-binding proteins (PBPs), which polymerize the glycan strands and crosslink the peptide side chains (Sauvage *et al.*, 2008). The PBPs are divided into two broad classes: Class A PBPs have both glycosyltransferase (GTase) and D,D-transpeptidase (TPase) activities, while Class B PBPs have only D,D-TPase activity (Sauvage *et al.*, 2008). Both activities are required for bacterial growth, during which there is a balance between new PG synthesis, and remodeling of existing PG (Typas *et al.*, 2012; Egan *et al.*, 2020). In contrast, PG remodeling is important for bacterial cell wall integrity (Morè *et al.*, 2019; Shaku *et al.*, 2020; Garde *et al.*, 2021). Some PG stem peptides are rapidly trimmed by D,D-carboxypeptidases to tetrapeptides (Peters *et al.*, 2016). While such tetrapeptides do not serve as substrates for PBPs, they can function as donors in reactions catalyzed by L,D-transpeptidases (LDTs), which produce 3–3 crosslinks between adjacent peptides (Shaku *et al.*, 2020; Garde *et al.*, 2021). The physiological role of LDTs is poorly understood; however, when persistently infecting fibroblasts in a nongrowing state, *Salmonella enterica* serovar Typhimurium increases the percentage of its cell-wall 3–3 crosslinking, which has led to the suggestion that host cues associated with a reduction in the bacterium's growth rate may stimulate LDT activity (Morè *et al.*, 2019; García-del Portillo, 2020).

We used synthetic fluorescent HCC-amino-D-alanine (HADA) and the dipeptide probe alkyne-D-alanine-D-alanine (EDADA) to study *V. fischeri* PG synthesis activity both in culture medium and within the light-organ crypts. For instance, HADA is incorporated into PG through the activities of PBPs and LDTs, thereby providing a way to track PG-transpeptidation activity (Kuru *et al.*, 2012; Hsu *et al.*, 2019). In contrast, we used EDADA to label more specifically at sites of new PG insertion only (Liechti *et al.*, 2014). In the cytoplasm, the ATP-dependent ligase MurF catalyzes the incorporation of D-Ala-D-Ala dipeptide into the UDP-*N*-acetylmuramic-acid-tripeptide to ultimately provide the precursor of new PG synthesis (Liechti *et al.*, 2014). The EDADA dipeptide mimics the D-Ala-D-Ala dipeptide in the reaction catalyzed by MurF and, thus, becomes incorporated into new PG in the place of D-Ala-D-Ala (Liechti *et al.*, 2014).

Here, we present evidence that PG biosynthesis by *V. fischeri* varies between the exponential and stationary phases of liquid cell culture, as well as within different crypts during the light-organ

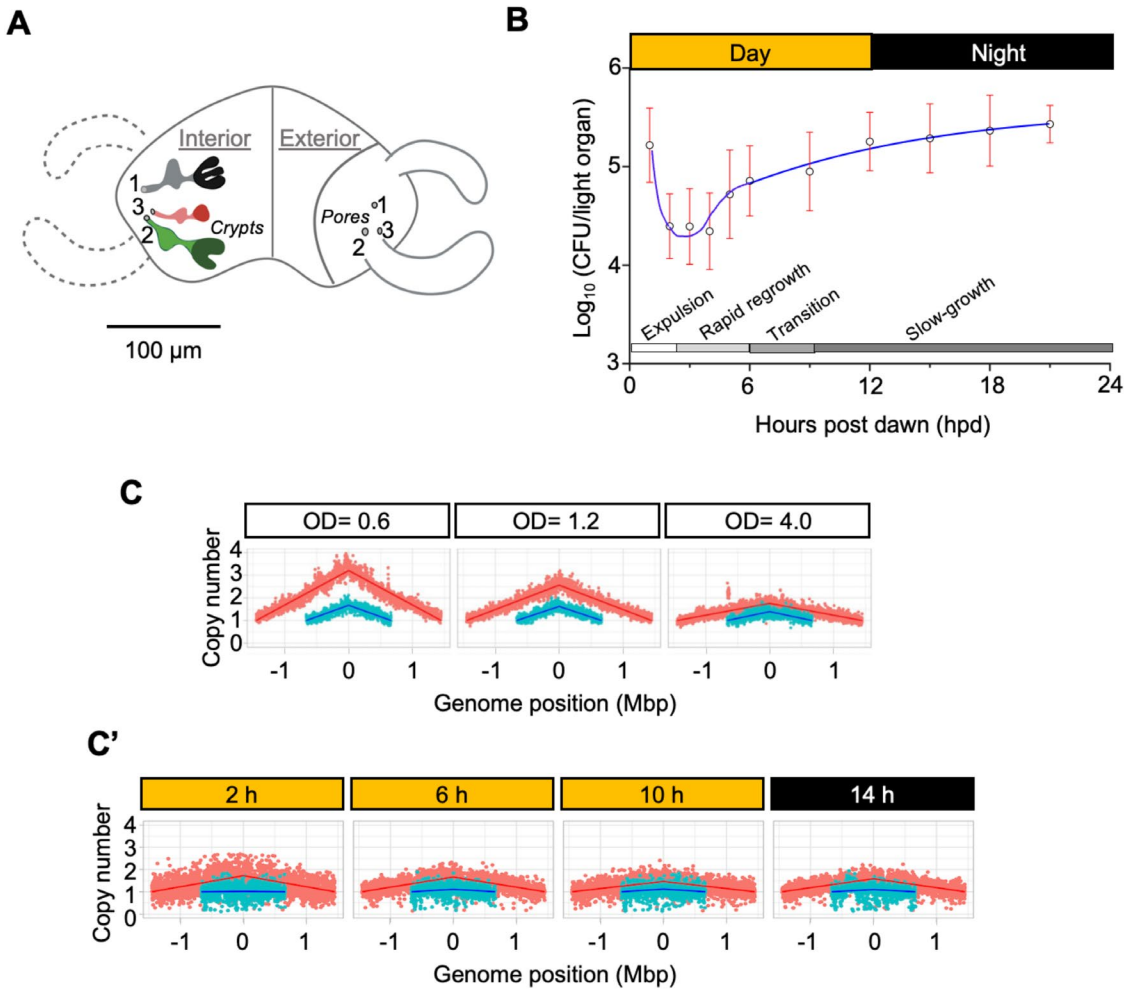

FIGURE 1: Initial colonization and the subsequent daily cycle of the *V. fischeri* symbiont populations. (A) Cartoon depicting the interior and exterior of the bilobed light organ of *E. scolopes*. Planktonic *V. fischeri* cells enter one of three pores on the external surface of both sides of the organ. Each pore leads to an independent epithelium-lined region (Crypt 1, 2, or 3) in which the symbionts grow and induce bioluminescence. In the cartoon, the crypts can be distinguished from the more distil antechamber regions by their darker color. (B) The number of colony-forming units (CFUs) in the light organ reflects the dawn-cued expulsion of most of the symbionts, followed by a rapid regrowth phase and a transition into a slow-growth, slow-growing phase (indicated by the bottom gradient bar). The black circles (and red lines) represent the mean CFUs (and the standard deviation; SD); $N = 30$ light organs from three individual clutches for each of 11 sampling points. Each clutch was treated as an independent experimental trial. A Shapiro-Wilk test was used to confirm that the data distribution adhered to a normal distribution. In addition, a one-way ANOVA was used to show no significant differences between the clutches for the data shown in Supplemental Figure S1B. A paired *t* test on log-transformed values of CFU/light organ measured between 1 hpd and 3 hpd demonstrated a statistically significant decrease, with a *p* value of 1.3×10^{-13}. Subsequent analysis of the CFU/light organ during the period between 3 and 6 hpd, applying a linear regression on log-transformed data, indicated a growth rate corresponding to a doubling time of 1.9 h, with an $R^2 = 0.81$, underscoring the model's efficacy in capturing the temporal dynamics of growth. (C) MFA diagrams indicating the number of copies of each gene along the length of the large (red) and small (blue) chromosomes of *V. fischeri* at three different ODs during an LBS-culture growth curve. The enrichment in the relative number of copies of genes located at the chromosomal origin (apex) decreases as the growth rate slows. (C') MFA data obtained from symbionts removed at 2, 6, 10, and 14 h post dawn (hpd). While the limited number of symbiont cells that could be collected from the juvenile light organs limited the precision of these measurements, the MFA patterns indicate that the population has a reduced growth rate at 10 and 14 hpd relative to that during regrowth (i.e., at 2 hpd).

symbiont's daily cycle of expulsion/regrowth. As predicted, in culture there was an upregulation in expression of an LDT (LdtA) only during the stationary phase, and in Crypt 1 only during the very slow-growth stage; however, LdtA was continuously upregulated in Crypt 3. These findings (i) offer important insights into how patterns of bacterial growth may differ depending on their tissue location, and (ii) have implications for our understanding how these differences influence the stability of longterm symbiotic relationships.

RESULTS

V. fischeri growth dynamics in the symbiosis show similarities to those in culture

With the exception of research focused on quorum-signaling and sporulation (Azimi *et al.*, 2020; Khanna *et al.*, 2020), our knowledge about bacterial growth dynamics during late-exponential and stationary phases is limited when compared with that of exponentially growing cells (Lupp and Ruby, 2005; Studer *et al.*, 2008;

Silva *et al.*, 2021; Lynch *et al.*, 2022). This information gap is particularly great when considering the growth of bacteria in animal tissues.

To determine the pattern of growth of *V. fischeri* within the juvenile light organ, we measured the number of CFUs present across a 24-h cycle beginning with the dawn expulsion event (Figures 1B; Supplemental Figure S1B). Earlier studies with adult *E. scolopes* had indicated that the expulsion of symbionts from the organ was largely completed within minutes of the dawn cue (Graf and Ruby, 1998): however, we found that in newly hatched juvenile squid the venting process was more gradual, decreasing the symbiont population ~10-fold over the first 3 h post dawn (hpd; *t* test, $p < 1.3 \times 10^{-13}$). After another 3–4 h, the number of CFUs had increased back to the typical ~10^5 level, with an apparent doubling time of ~1.9 h ($R^2 = 0.81$). Intriguingly, during the following 18 h, a period we term the very slow-growth phase, the CFUs showed only a minimal increase (~1 doubling), suggesting a severe reduction in the symbiont's metabolic activity. However, this slow-growth phase extended into and throughout the night (Figure 1B), the period when the symbiont's bioluminescence output is typically at its highest (Ruby and Asato, 1993; Boettcher *et al.*, 1996), thus indicating the maintenance of a significant catabolic activity without a concomitant growth in biomass.

Because the number of CFUs is a measure of a bacterial population's net proliferation (i.e., a high proliferation rate can be masked by a concurrent loss in viability), we asked whether there was evidence that the intrinsic growth rate of the symbionts is actually reduced during the night. Specifically, we used a molecular approach to estimate the index of replication (*iRep*) using marker-frequency analysis as an indication of the symbiont's average instantaneous rate of growth (Skovgaard *et al.*, 2011; Brown *et al.*, 2016; Val *et al.*, 2016; Higgins *et al.*, 2022). Briefly, when the bacteria are growing rapidly (e.g., exponential phase), the ratio of the number of gene copies at the genome's origin to that at the terminus is three to four; in contrast, at a slow growth rate (e.g., stationary phase), that ratio is closer to one (Figure 1C). When symbionts were collected directly from the light organ at different times of day and immediately analyzed, the apparent growth rate during the very slow-growth period was reduced by a factor of at least two relative to their maximum (Figure 1C'), consistent with the reduction in growth rate beginning ~ 6 h after dawn as indicated by the CFU levels (Figure 1B).

Cell division activities change during the growth of *V. fischeri*

Cell division is central to bacterial growth dynamics, yet standard measures like OD and CFU fall short in capturing these intricate *processes* (Roller *et al.*, 2023). To bridge this gap, we investigated these two processes in *V. fischeri* at different stages of population growth, first in cell culture, and then during symbiosis, using fluorescent indicators of the cell-division machinery.

We first localized the divisome in cultured *V. fischeri* cells using an mCherry fusion protein linked to the cell-division marker ZapA, a critical component of this process. Inspection of growing cells by fluorescence microscopy indicated that the divisome was present at the midline of predivision cells, and at the pole of each daughter cell, as reported for *Vibrio cholerae* (Galli *et al.*, 2017). This localization was evident in demographs constructed from analyses of rapidly growing cells (i.e., OD 0.5) (Figure 2A). However, as the bacterial culture increased in OD above 1.0, both the intensity of the ZapA-mCherry marker and its confinement to the midline diminished significantly (Supplemental Figure S2), consistent with a reduced activity of the cell-division machinery as the cells exited the exponential phase.

To explore the relationship between cell division and bacterial PG transpeptidation activity, we introduced a PG-specific fluorescent D-amino acid (HADA) precursor for cell wall crosslinking to the bacterial culture for 5 min (~ 10% of the exponential doubling time). The resulting HADA signal colocalized with the ZapA-mCherry marker (Figure 2B), which indicated that there is a concentration of PG-synthesizing transpeptidases at the site of septum formation and cell division in rapidly growing cells.

Variations in HADA labeling suggest changes in PG transpeptidation activity throughout bacterial growth

Given the variability *between* growth phases, and the weakening of the ZapA-mCherry signal during stationary phase, we investigated whether HADA incorporation changes as the growth rate slows. When cultures of *V. fischeri* cells were incubated with HADA, at an OD of 2.0 or higher, the labeling pattern was no longer concentrated at the midline; instead, most cells began to show a more random pattern of labeling throughout the cell (Figures 3A; Supplemental Figure S3). To better ascertain the location of new PG insertion throughout growth, bacterial cultures at different ODs were briefly labeled with EDADA (Liechti *et al.*, 2014), which specifically marks sites of new PG synthesis (Supplemental Figure S4). While the overall extent of labeling slowed as cells approached stationary phase, the appearance of new PG continued to be confined to the midcell, irrespective of the stage of growth.

HADA labeling during exponential growth appears to primarily reflect new PG synthesis, likely facilitated by PBPs (Liechti *et al.*, 2014; Hsu *et al.*, 2019). However, as the cells approach stationary phase, HADA incorporation suggested a shift to more complex activities, with labeling patterns dispersing beginning at an OD of ~2 (Supplemental Figure S3), This shift accompanies a >fivefold decline between OD 0.5 and 6 (Figure 3B), suggesting a gradual reduction in HADA *assimilation* into PG networks after OD 0.5. This finding also reflects a decrease in PG transpeptidation activity as bacteria transition into the stationary phase, coincident with a decreasing cell volume (Figure 3C) and a reduction in cell-division machinery, suggesting that while PG transpeptidation is active during the early exponential phase, it diminishes as cells progress into the stationary phase, coinciding with the slowing of cell division.

To further examine the dynamics of HADA incorporation, we conducted a saturation labeling followed by a no-label chase. Specifically, *V. fischeri* cells were labeled with HADA for a period equivalent to two doubling times, washed, and then transferred to label-free medium to measure any loss of fluorescent signal as they continued to grow (Figures 4; Supplemental Figure S4). During the early exponential phase (OD 0.5), the greatest loss of fluorescent signal may potentially be due to the insertion of new PG during elongation and/or to a uniform level of turnover of the labeled PG by hydrolysis. In contrast, during stationary phase (OD 4.0), the bacteria displayed a minimal level of growth, leading to a decrease in *fluorescent* intensity throughout the entire cell. Both the short-term HADA labeling (Figure 3A) and the loss of fluorescent intensity at the midcell during this experiment support the hypothesis that HADA incorporation diminishes as the cell progresses into the stationary phase or a stage of very slow division. This conclusion is further evidenced by the pattern of ZapA-mCherry labeling, suggesting that PG-transpeptidase activity by symbionts becomes more varied and complex when they are in the slow-growth phase.

The pattern of PG synthesis within host tissue mirrors that occurring in culture

We next sought to *determine* the patterns of PG synthesis when symbionts colonize the light-organ crypts. To examine growth in the symbiotic environment, we first focused on the largest and most

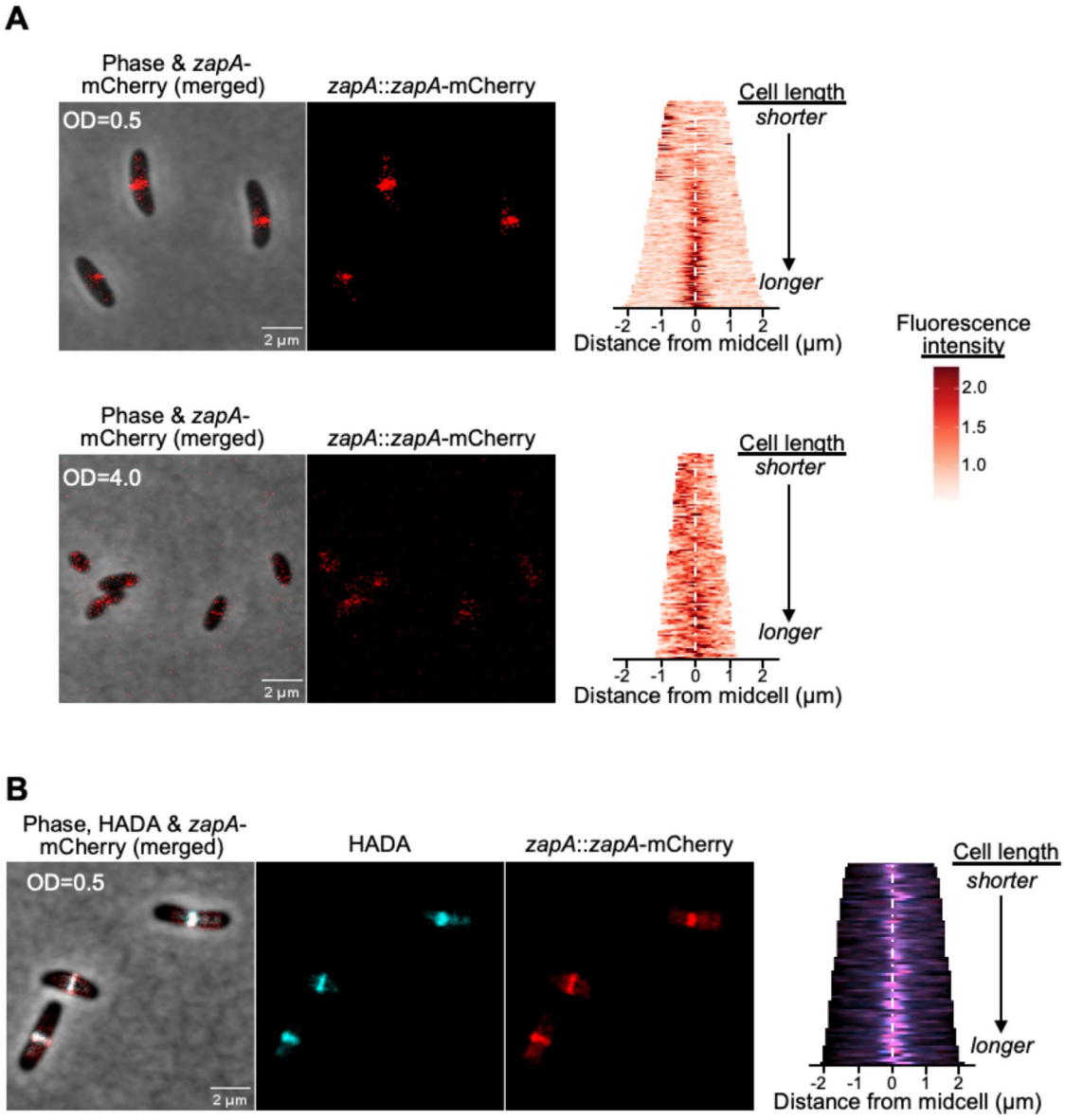

FIGURE 2: Activity of the *V. fischeri* cell division machinery decreases as the cells transition into stationary phase. (A) Representative phase micrographs showing the midcell position of the cell-division protein ZapA (ZapA-mCherry; red). Quantitative analyses of the ZapA-mCherry fluorescence localization, shown as demographs, at two OD values of a wild-type *V. fischeri* strain ES114 culture. The demograph is used to illustrate the fluorescence profiles of the population using a randomly chosen set of cells, where single-cell fluorescence profiles are sorted by cell length and stacked to generate the graph. The middle of the cells is indicated by a white dashed line. Scale bar = 2 μm. (B) ZapA-mCherry colocalizes with sites of new PG synthesis; Left, representative images of *V. fischeri* ZapA-mCherry cells at OD 0.5 that were briefly labeled with 1 mM HADA (cyan). Scale bar = 2 μm; Right, the fluorescence signal of HADA (cyan) and ZapA-mCherry (red) in each individual cell was quantitatively analyzed and their colocalization demonstrated in a demograph.

mature pair of crypts (Crypt 1; Figure 1A). Colonized squid were briefly incubated with HADA for 1 h, and then fixed before fluorescence imaging of the light organ. We analyzed time points that represented the three daily stages of the symbiosis: the regrowth phase (2–6 h post dawn; hpd), the transition phase (6–9 hpd), and the slow-growth phase (9–24 hpd; Figure 1B). During the regrowth phase (4 hpd), we observed midcell labeling of the bacteria, while in the slow-growth phase (10 hpd), the labeling pattern of the symbionts was random around the cell wall (Figure 5A). Not surprisingly, during the transition phase there was a mixed pattern, with some cells showing midcell labeling and others showing random labeling (Supplemental Figure S6A). Based on HADA incorporation in culture, we concluded that during the regrowth phase, cells are rapidly dividing, while during the slow-growth phase, they divide only once or twice in 12 h. Moreover, we found that the amount of HADA associated with the cell wall decreased once the symbiont had left the growth phase (Figure 5B). This decrease in cell-associated fluorescence beginning at 6 hpd supports the conclusion based on CFUs (Figure 1B) that cell growth/division slows significantly after that point.

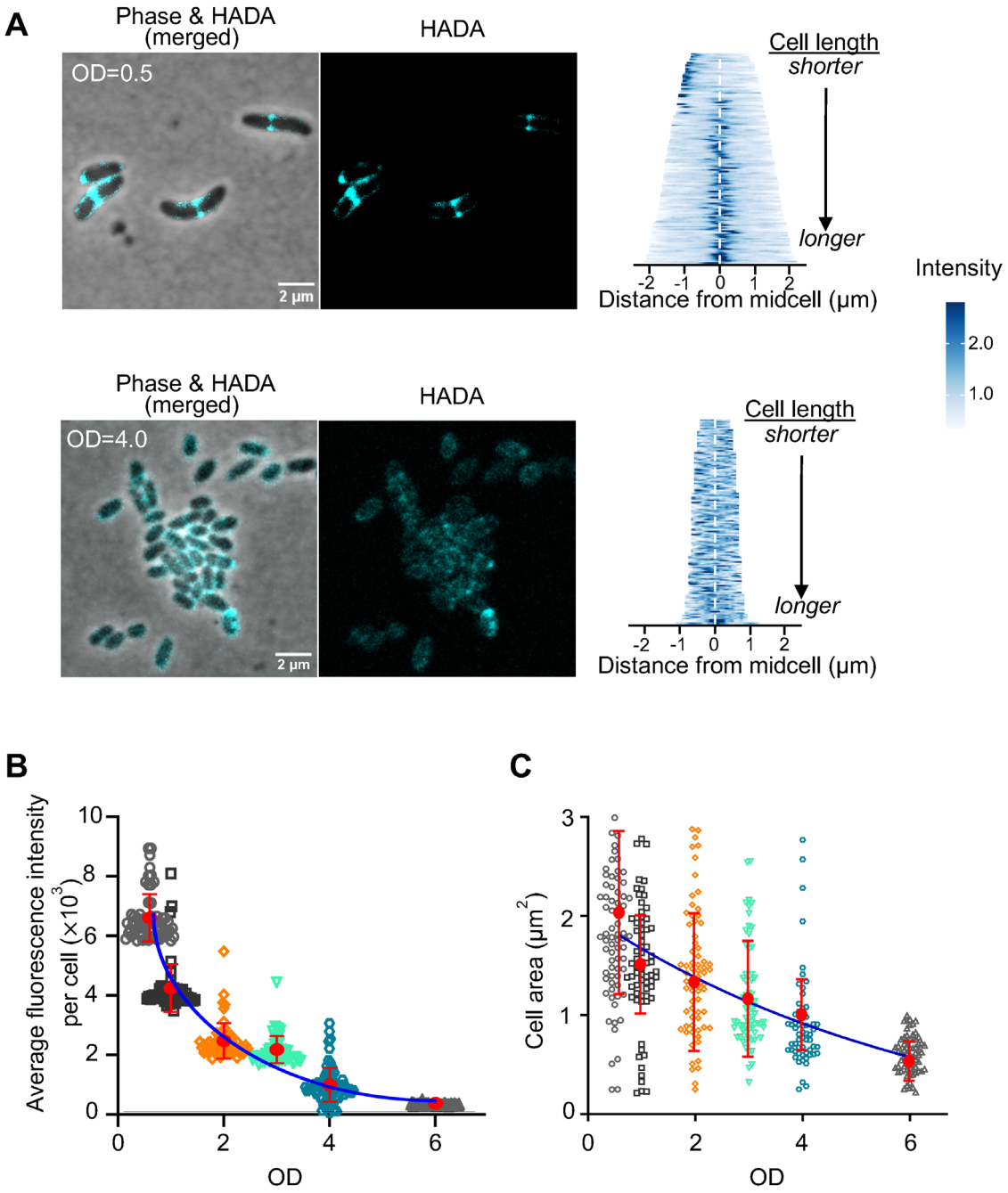

FIGURE 3: HADA-labeling patterns vary at different culture densities in *V. fischeri*. (A) Short-term HADA labeling of strain ES114. Left, representative phase micrographs of cells from cultures at two OD values that were fluorescently labeled with 0.5 mM HADA (cyan). Scale bar = 2 μm. Right, demographs quantifying the cellular location of HADA labeling in *V. fischeri* cells from the culture imaged on the left. The middle of the cells is indicated by a white dashed line. (B) Quantification of the average fluorescence intensity in cells that were pulse-labeled with HADA at different OD values. The fluorescence intensity at each OD was distinguished using distinct colors in the scatter plot, with each dot representing an individual cell. The red circle represents the mean fluorescence intensity at each OD, while the red line represents ± one SD; $N = 80$ for all points. The blue line shows the fitted curve. (C) Size (approximated by cross-sectional area) of *V. fischeri* cells from a culture at different OD values; the red circle indicates the mean and the red line indicates ± one SD; $N = 80$ for all points. The blue line shows the fitted curve.

The microbiogeography of host tissues affects the dynamics of PG synthesis

During the *embryological* development of *E. scolopes*, the sequential formation of light-organ crypts results at hatching in the presence of three sets of crypts of different sizes (Montgomery and McFall-Ngai, 1993) and levels of maturity (Essock-Burns *et al.*, 2020, 2023). Notably, for the first few days posthatch, the least mature Crypt 3 does not vent its symbiont population as Crypts 1 and 2 do (Essock-Burns *et al.*, 2023). This delay suggests that the symbionts in Crypt 3 do not experience the diurnal reduction in population density that is characteristic of the more mature crypts. Thus, using a HADA-labeling approach, we asked whether there was evidence of

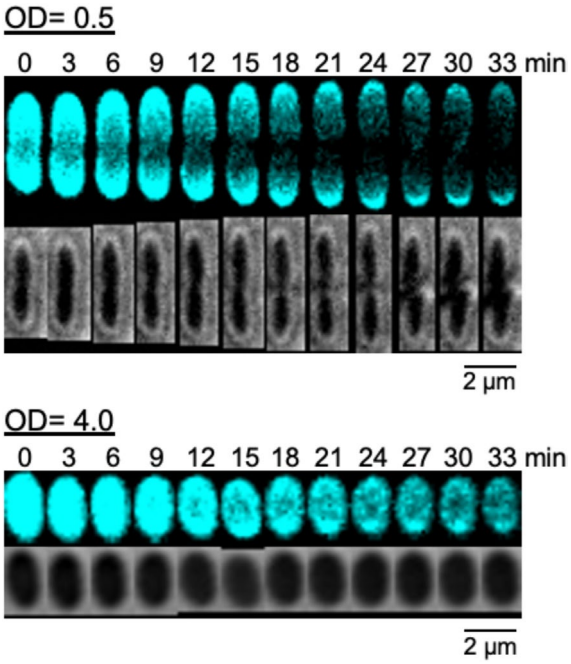

FIGURE 4: Time-lapse analysis of individual *V. fischeri* cells taken from an LBS culture at two ODs. The cells were uniformly labeled with 1 mM HADA (cyan), followed by washing, transferring to glass slides, and mounting on pads saturated with LBS containing 1.5% agarose, without additional HADA label. Imaging of the cells was performed at 3-min intervals for a period of 33 min.

a daily cycle alternating between rapid growth and very slow proliferation by the symbionts within Crypt 3. Images were captured at two time-points: 4 and 10 h postdawn (Figure 1B). Even at 4 hpd, most of the symbionts in Crypt 3 did not display midcell labeling, with the exception of a few that were nearest the crypt epithelium (Figures 5A′; Supplemental Figure S6B) where the bacteria and host are most likely to give/receive signals or nutrients. Moreover, at both time points, those few cells displayed a significantly greater fluorescence intensity compared with symbionts that were further from the host epithelium, a microbiogeographic pattern of labeling that was not observed among the symbionts in Crypt 1 (Figure 5C). Taken together, these findings demonstrate that symbionts in Crypt 3 exhibit different patterns of PG synthesis and therefore, at least from the standpoint of PG synthesis, may inhabit a more heterogeneous environment than their counterparts in Crypt 1.

The temporal expression pattern of LDTs reflects tissue maturity

Using NanoString *analysis*, a direct, molecular barcoding method that quantifies the abundance of RNA transcripts accurately and efficiently without amplification (Levy *et al.*, 2018), we found elevated *ldtA* transcript levels in the light-organ symbionts during the slow-growth phase (i.e., 0400, 1600, and 2200 h) compared with the regrowth phase (i.e., 1000 h; Figure 6B). To better understand the timing and location of *ldtA* expression and, by extension, the onset of cell-wall modification, we visualized the presence of *V. fischeri ldtA* mRNA using hybridization chain-reaction fluorescence in situ labeling (HCR). This method allowed us to compare the expression levels of *ldtA* in bacteria: (i) during exponential and stationary phases in culture medium, as well as during the regrowth and slow-growth stages in the light organ, and (ii) within different crypt environments (i.e., Crypt 1 and Crypt 3). We found that, while *ldtA* mRNA was not detected in cultured cells during exponential phase, it was broadly expressed during stationary phase (Supplemental Figure S7A). No *ldtA* mRNA was observed in the Δ*ldtA* strain (Supplemental Figure S7B), supporting the specificity of the HCR probes.

As predicted, HCR imaging did not detect *ldtA* mRNA in the bacteria within Crypt 1 during the daily regrowth phase (4 hpd) of the symbiosis; however, its expression became evident once the population had entered the slow-growth stage (10 hpd; Figure 6A). In contrast, Crypt 3 symbionts showed robust *ldtA* expression throughout the diurnal cycle. This differential expression suggests unique PG synthesis dynamics depending on the development state of the host tissue. Specifically, after their initial colonization event, symbionts in the less mature Crypt 3 appear to primarily undergo PG remodeling, while those in Crypt 1 engage in this process only during the slow-growth stage that occurs as part of the diurnal cycle. Because Crypts 1 and 3 contain 84 and 2%, respectively, of the juvenile light organ's symbionts (Montgomery and McFall-Ngai, 1993), it is not surprising that the level of *ldtA* transcript detected by NanoString analysis reflected the images of Crypt 1: lowest during the postdawn regrowth period, and increasing as the population entered the slow-growth stage (Figure 6B). As expected, in juvenile squid colonized with a Δ*ldtA* mutant, no *ldtA* mRNA signal was observed using HCR (Supplemental Figure S8).

Carriage of *ldtA* provides a competitive advantage during symbiosis

Given the rhythmic expression of *ldtA* by Crypt 1 symbionts, we investigated whether carriage of this gene might play a role in successful *persistence* in the association. The Δ*ldtA* mutant grew as well as its wild-type parent in culture medium (Supplemental Figure S9A). Furthermore, during the initial 4 d of colonization, the mutant showed a similar level of persistence within the light organ as its wild-type parent (Supplemental Figure S9B). These data suggested that LdtA was not essential for normal growth or colonization. However, when competing in a coinoculation with its parent, the Δ*ldtA* strain demonstrated a marked decrease in competitive persistence after 48 h (Figure 7A), with the parent strain surpassing Δ*ldtA* by as much as a factor of 10 at 96 h. Nevertheless, over the first 4 d of the symbiosis the luminescence per CFU in the colonized squid remained stable (Figure 7B), suggesting that together the wild-type and mutant strains continued to be both metabolically active and capable of maintaining a high level of luminescence.

DISCUSSION

Many studies have examined how beneficial bacteria initially colonize host tissue. However, there is a much more limited understanding of the mechanisms employed by these symbionts for their subsequent proliferation and maintenance (Koch *et al.*, 2014; Bergkessel and Delavaine, 2021). In this report, we posit that during the periods of slow or no growth that often characterize the persistence of such associations, symbiotic bacteria change the nature of their PG synthesis activities, and that these changes are important for their long-term survival. To test this hypothesis, we described and compared the patterns of PG synthesis of *V. fischeri* growing in laboratory culture to those of *V. fischeri* cells inhabiting the light organ of its sepiolid squid host, and asked whether those activities underlie a successful symbiosis. To understand the mechanisms driving the daily PG dynamics in the symbiosis, we used two fluorescently labeled noncanonical D-amino acids (HADA and EDADA) in an effort to determine whether PG synthesis varies between rapid- and slow-growth phases. Our findings revealed that the pattern of

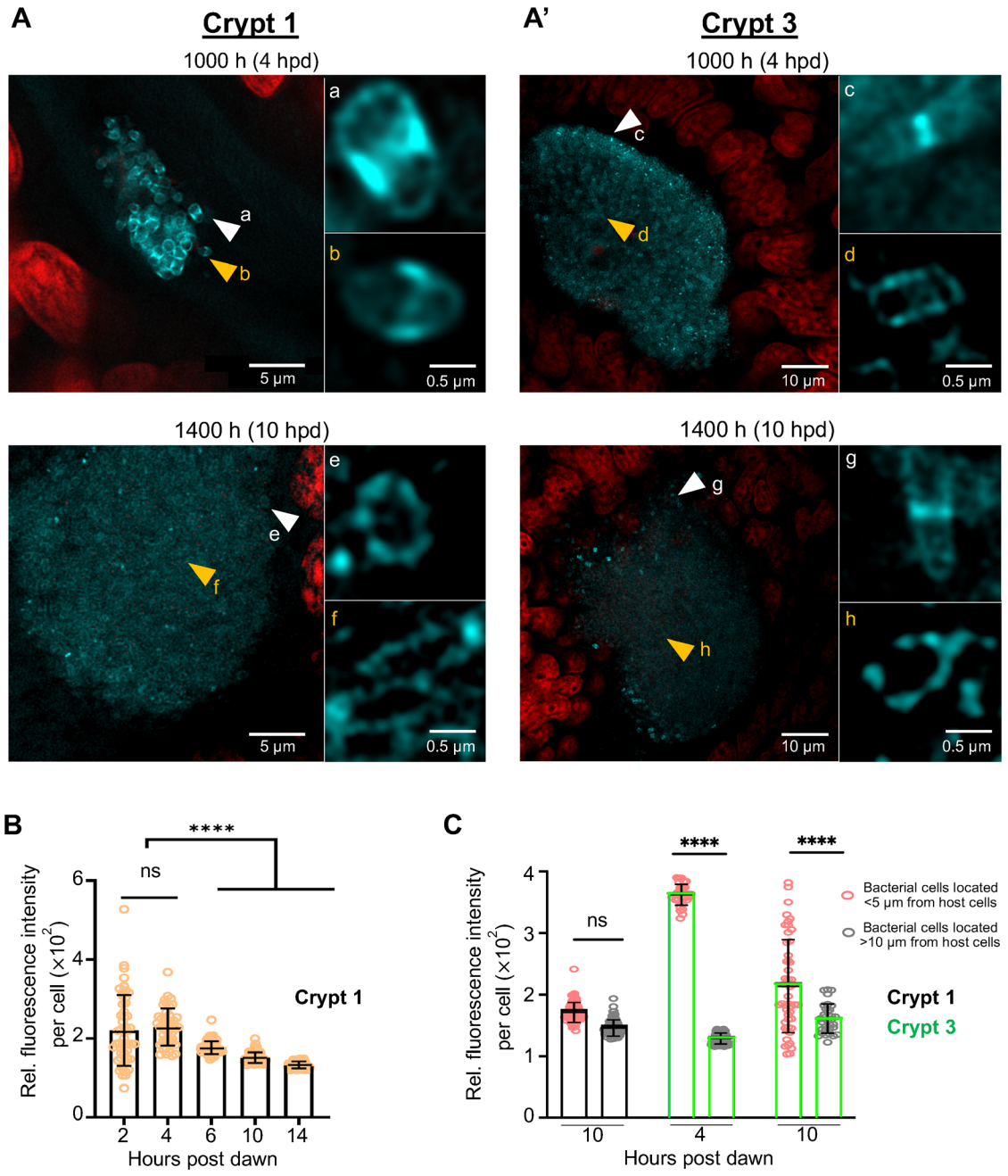

FIGURE 5: The dynamics of PG synthesis by *V. fischeri* symbionts at two times during the light organ's daily cycle. (A, A') Fluorescence microscopy images of symbiont-colonized crypts at two times after the dawn light cue (hpd = hours post dawn). Samples were treated at the indicated times with HADA (cyan) for 1 h to localize its incorporation into PG. Cell nuclei were counterstained using TO-PRO-3 (red). Insets provide a higher magnification of the bacterial cells indicated by arrows (a-h); white arrows point to bacteria adjacent to host cells, while yellow arrows indicate bacteria distant from host cells. (B) Analysis of per-cell fluorescence intensity of *V. fischeri* symbionts within Crypt 1, derived from images in panel (A) and Supplemental Figure S5. Data were collected at five different times in the diel cycle. (C) Analysis of per-cell fluorescence intensity of *V. fischeri* symbionts within Crypts 1 or 3 at two time points, as a function of their proximity to host cells lining the crypts. Data collection was limited to time points when the crypts were fully colonized (Crypt 1 was excluded from consideration at 4 hpd because it was not recolonized by this time). Each point denotes an individual biological replicate. TO-PRO-3 staining was used to segment bacterial cell nuclei, with the stain's brightness adjusted to exclusively highlight the host cells. The black lines indicate the mean and the SD. Statistical significance was assessed using Mann-Whitney U tests, where **** denotes $P < 0.0001$, and "ns" indicates not significantly different.

HADA labeling undergoes a change as cells transition into very slow-growth, and this change correlates with ZapA-mCherry localization. Concurrently, EDADA labeling indicated that the insertion of new PG remains relatively constant throughout the growth cycle. Together, these observations indicate a distinct difference in PG synthesis between rapid and slow phases of growth.

During our analyses of *V. fischeri* in lab culture we observed that, despite the graphical indications of an apparent balanced growth

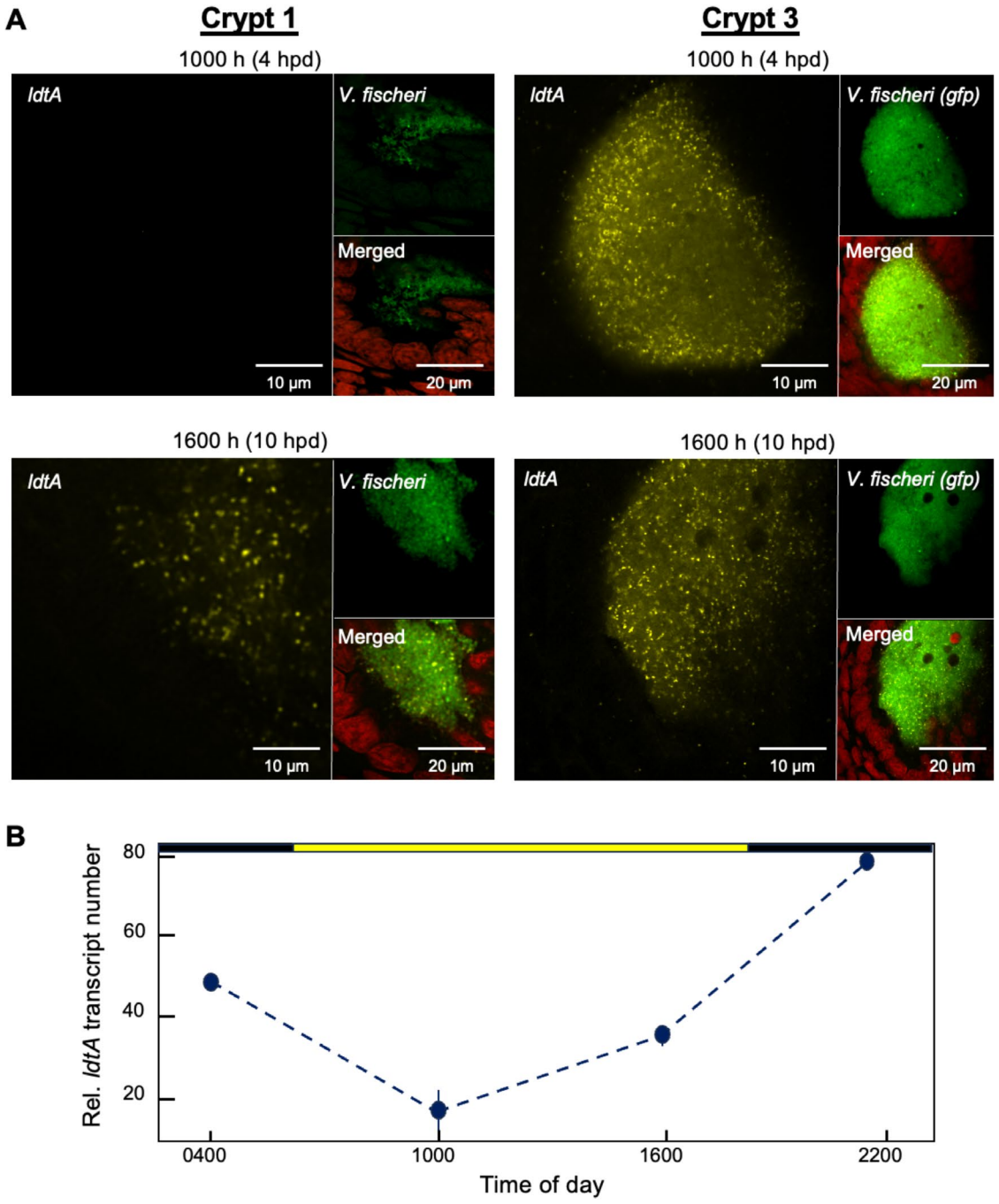

FIGURE 6: Expression of *V. fischeri ldtA* in the light organ, depending on time and crypt. (A) Transcripts of *ldtA* (gold) were localized in juvenile light-organ crypts using HCR of GFP-labeled *V. fischeri* (green). Expression of *ldtA* by *V. fischeri* within Crypts 1 or 3, was determined at either 4 or 10 h post dawn (hpd). Nuclei of the crypt epithelia were stained with TO-PRO-3 (red). (B) The relative number of *ldtA* transcripts in the entire symbiont population (normalized to total mRNA) over a daily cycle of expulsion and regrowth, as measured by NanoString nCounter analysis.

between ODs of 0.5 to 4.0 (Supplemental Figure S1), the pattern of PG synthesis changes markedly even though the culture is growing exponentially. Specifically, while cell division and new PG insertion are initially synchronized, as evidenced by the colocalization of ZapA and HADA (Figure 2B), when culture growth progresses beyond an OD of 2.0, a marked decline in the initiation of cell division occurs, coincident with a dispersal of ZapA and a reduced HADA labeling at the midcell (Supplemental Figures S2 and S3). These findings underline the limitations of relying on CFU or OD measurements to infer that a complex process like cell division or PG synthesis is proceeding unchanged. In fact, our results lead us to conclude that in culture a truly balanced period of growth and cell division in *V. fischeri* is briefer than predicted and, consistent with what has recently been reported in *Escherichia coli* (Sezonov *et al.*, 2007; Roller *et al.*, 2023), does not actually encompass what is typically considered the characteristics of an exponential phase.

Natural environments often expose bacteria to conditions that produce a reduced growth rate, typically marked by nutrient

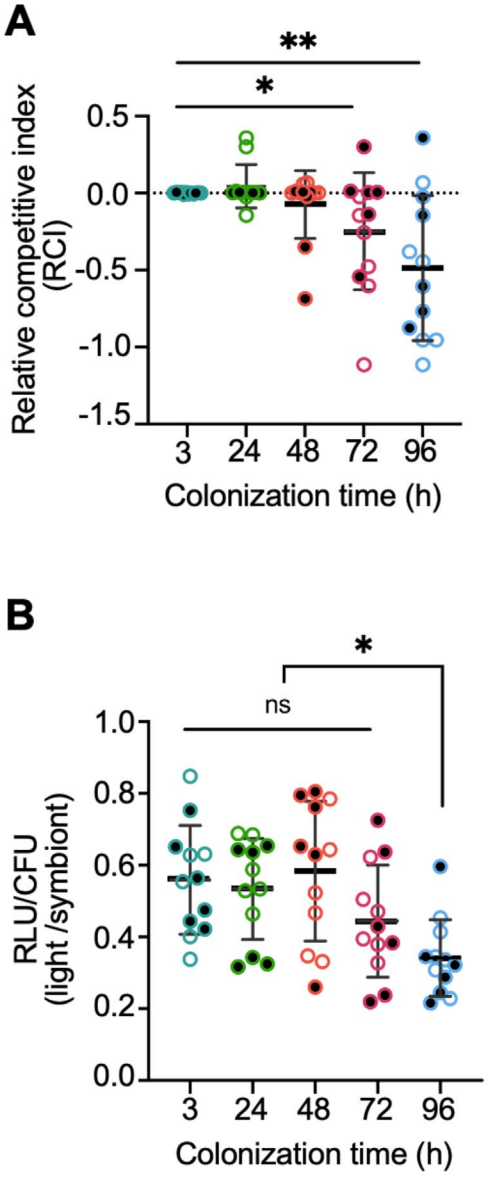

FIGURE 7: Competitive colonization dynamics in *E. scolopes* between *V. fischeri* wild-type and Δ*ldtA* mutant strains. Hatchling squid were exposed to a concentration of 4×10^3 CFU/mL a 1:1 mixture of either: (i) the Δ*ldtA* mutant tagged with an RFP-encoding plasmid (pVSV208), and unmarked wild-type *V. fischeri* (solid circles); or, (ii) the unmarked Δ*ldtA* mutant, and wild type tagged with the RFP-encoding plasmid (open circles). Postinoculation, the squid were rinsed daily in fresh *V. fischeri*-free seawater, and the persistence of their symbiosis assessed by determining their luminescence. (A) RCI was determined as described in the *Materials and Methods*. Each point reflects the RCI obtained from a single juvenile. (B) Relative luminescence units (RLU) per CFU were used to quantify the bioluminescence from squid light organs colonized by the mixed population of wild-type and Δ*ldtA* strains. Each data point corresponds to an individual squid. Error bars signify ± the SD.

deficiencies and suboptimal pH or other biochemical stresses (Bergkessel *et al.*, 2016; Stapels *et al.*, 2018; Yin *et al.*, 2019; Wheatley *et al.*, 2020). Our data indicate that, during very slow growth or stationary phase, *V. fischeri* upregulates *ldtA*, which encodes a PG-modifying LDTs (Figures 6; Supplemental Figure S6A). Two of the LDTs of *E. coli* (YcbB and YnhG) produce 3–3 crosslinks in the PG, remodeling the cell wall and making it more stress resistant (Alvarez *et al.*, 2021). In contrast, *Vibrio cholerae* encodes only one enzyme (LdtA) that is responsible for 3–3 crosslinking (Alvarez *et al.*, 2021). The LdtA of *V. fischeri* (designated VF_1157) has 87% amino-acid sequence similarity to the *V. cholerae* ortholog; however, whether it provides the only 3–3 crosslinking activity to *V. fischeri* as well is unknown.

LdtA expression by *V. fischeri*, both in cell culture and in the light organ, is increased during periods of slow growth. Similarly, when in the phagosome, *S. typhimurium* upregulates a specific PBP that is effective solely in an acidic environment, thereby promoting bacterial division and survival within that stressful host compartment (Castanheira *et al.*, 2017). Surprisingly, Reed *et al.* (2015) managed to eliminate most genes encoding transglycosylase- or transpeptidase-domain enzymes in *Staphylococcus aureus*. While this extensive deletion of PG machinery did not produce a growth phenotype in culture, in host infection studies the mutant displayed an increased antibiotic susceptibility and decreased virulence. Such findings hint at the possibility that reliance on results of cells grown under laboratory conditions might obscure enzyme activities or PG-structural variations that are most relevant in natural growth settings like host tissues. We postulate that the activity of *V. fischeri* LdtA in slow-growing symbionts could be crucial for maintaining cellular stability under certain host-tissue conditions, as reported for bacteria as diverse as *E. coli* and *Mycobacterium tuberculosis* (Pisabarro *et al.*, 1985; Squeglia *et al.*, 2018; Gokulan and Varughese, 2019; Papadopoulos *et al.*, 2021). Such a diminished cell stability could explain the colonization defect of a Δ*ldtA* mutant (Figure 7A). Another possible reason for the symbiosis defect in the absence of LdtA relates to the role of this *V. cholerae* enzyme in recycling free PG tetrapeptide monomer (termed TCT) that would otherwise accumulate in the periplasm (Alvarez *et al.*, 2021). Because this molecule is a potent inducer of developmental events in the juvenile squid (Koropatnick *et al.*, 2004), colonization by a mutant that releases an increased level of TCT signal might imbalance the communication between the partners (Adin *et al.*, 2009). To test these hypotheses, more comprehensive PG structural studies are needed that focus on the effect of different growth rates on the expression and products of PG synthesis and modifying enzymes, and on the resultant PG structures they create in symbionts (Alvarez *et al.*, 2021).

As cells transition from rapid growth, in either culture or within host tissue, *V. fischeri* encounters environmental challenges that could elicit changes in PG-synthesis activities. During the daily cycle of symbiosis (Figure 1B), factors such as nutrient limitation, toxin accumulation, or space constraints may periodically become influential (Schwartzman and Ruby, 2016). Because the pattern of fluorescent labeling changes with the level of bacterial occupation in the crypts, we asked what role spatial constraints within the crypts might play in modulating symbiont PG synthesis. Prior research has shown that, compared with its wild-type parent, a nutritional auxotroph of *V. fischeri*, Δ*lysA,* can colonize only ~10% of the available crypt space within the light organ due to a lysine limitation (Aschtgen *et al.*, 2016; Essock-Burns *et al.*, 2020). Nevertheless, this mutant exhibited both a similar cellular distribution of PG labeling and a pattern of decreasing fluorescence per cell over time as wild type (Figure 5B), even though the mutant population had not fully occupied the major crypt and still had space in which to expand (Supplemental Figure S10). These results suggest that a symbiont's growth isn't limited by either the availability of crypt space or by a condition (like acidification or oxygen limitation) that is directly related to population size; instead, growth limitation may be determined simply by the amount of nutrients that the host tissues of each crypt provide (Graf and Ruby, 1998).

Another intriguing observation from this study was the distinct behavior of the symbionts in Crypt 3 when compared with the bacteria in the more mature Crypt 1; specifically, while in Crypt 1 *ldtA* is only highly expressed at night, it is expressed in Crypt 3 during both the morning and night (Figure 6), a result that is consistent with the apparent absence of growth of the majority of symbionts in Crypt 3 throughout the day (Essock-Burns *et al.*, 2023). This difference in expression over the day/night cycle also underscores how the induction of functionally specific PG enzymes may be different in distinct tissue compartments. A recent report found that *V. fischeri* cells colonizing Crypt 3 exhibit resilience against external factors like antibiotic intervention, potentially due to its more metabolically-inactive symbiont population (Essock-Burns *et al.*, 2020, 2023), a conclusion that aligns with the pattern of *ldtA* expression. These data point to a distinct, and likely more stressful, microenvironment in Crypt 3 that reflects the presence of diverse bacterial-host interactions within the different crypts (Essock-Burns *et al.*, 2023). Alternatively, the developmental dynamics within Crypt 3 tissues may inhibit bacterial expulsion, thereby maintaining the crypt inhabitants in a prolonged stationary phase–a state known to confer cross-resistance to multiple stresses. Future research will aim to: (i) further elucidate these microbiogeographical differences and their implications for host development and symbiont persistence, and (ii) experimentally alter the expulsion cycle in Crypt 3 to determine its effects on symbiont growth dynamics. The colonization dynamics within the light organ suggest parallels with the mammalian microbiome, wherein the developmental state of gut tissues plays a pivotal role in shaping their associated microbiota (Stewart *et al.*, 2018). Similarly, the persistence of microbiome colonization in the gut, along with the periodicity in transcriptional activities currently being revealed (Daas and de Roos, 2021; Goh *et al.*, 2021; Frazier and Leone, 2022) suggests that successfully managing the growth of their microbial partners over time is a common theme in phylogenetically diverse animals.

MATERIALS AND METHODS

Bacterial strains and growth conditions

Strains and plasmids used in this study are summarized in Table S1. *E. coli* was grown in lysogeny broth (LB) at 37°C (Bertani, 1951); *V. fischeri* was grown in LB-salt (LBS) medium at 28°C (Bennett *et al.*, 2020). Overnight cultures were inoculated with single colonies from freshly streaked -80°C stocks. Liquid cultures were shaken at 225 rpm. When appropriate, antibiotics were added to overnight cultures at the following concentrations: kanamycin (Km), 50 µg/ml; chloramphenicol (Cm), 5 µg/ml (for *V. fischeri*) or 25 µg/ml (for *E. coli*). Experimental cultures of *V. fischeri* were grown in seawater-tryptone (SWT) medium at 28°C (Boettcher and Ruby, 1990).

To monitor bacterial growth, the optical density (OD) of cell suspensions was determined spectrophotometrically at 600 nm. At an OD above 1.0, the cell suspension was diluted 10-fold before taking a measurement. Colony counts were performed by serial 10-fold dilutions in LBS, after adjustment of the concentration based on OD. Aliquots of 50 µl of each sample were plated onto LBS agar, and incubated for 18 h.

Plasmid and mutant construction

Primers used to construct the deletion and expression vectors in this study are listed in Supplemental Table S1. In-frame deletion of genes in the *V. fischeri* genome was performed as previously described (Bennett *et al.*, 2020). Counterselection to remove the target gene and pSMV3 was performed on LB-sucrose (per liter: 2.5 g NaCl, 10 g Bacto-Tryptone, 5 g yeast extract, 100 g sucrose) for 2 d at room temperature. The pSMV3-derived plasmids were integrated into the bacterial chromosome by single-homologous recombination at the *zapA* locus. Gene replacement was achieved by double-homologous recombination using the counter-selectable *sacB* marker. Proper chromosomal integration or gene replacement was verified by colony PCR and sequencing.

Colonization assay

V. fischeri strains were grown at 28°C overnight in LBS medium supplemented with either Cm or Kn depending on whether they were carrying a resistance marker (Supplemental Table S1). The overnight cultures were diluted 100-fold in SWT broth, and grown until mid-exponential phase at 28°C. Cultures were diluted to a final concentration aimed at providing an inoculum of ~5,000 CFU/ml in 100 ml of 0.2-µm pore-size filtered-sterilized ocean water (FSOW), into which newly hatched juvenile *E. scolopes* squid were placed. After a 12-h exposure to the inoculum, each squid was transferred to a vial containing 5-ml FSOW, and incubated overnight in a room with a 12-h/12-h day/night cycle. After 36 h post inoculation (hpi), the squid were killed and frozen at -80°C in 700 µl of FSOW for 1 h to eliminate surface contaminants before being thawed and individually homogenized. Dilutions of the homogenate were spread on LBS agar medium, and the number of CFU/light organ was calculated.

To determine the dynamics underlying the daily expulsion and regrowth of the symbiont population, three replicate experiments were conducted. Each of the three groups of 110 juvenile animals originated from a separate clutch of eggs laid by a different adult female, on three different days. We treated data from each clutch as an independent experiment. In each of these three replicates, at 11 time points during the day, 10 animals were analyzed. This approach tests the reproducibility of the results. In addition, the data from the three replicates were combined to provide a higher degree of rigor (i.e., 30 animals per time point over 11 timepoints) in the display. These approaches were adopted to ensure that the variability among clutches could be embraced in our analysis, thereby enhancing the ecological relevance of our findings.

Squid competitive colonization assay

V. fischeri strains (wild-type and Δ*ldtA*) were cultured overnight in liquid LBS at 28°C, then diluted 1:100 in SWT broth, and grown until they reached an OD of ~ 0.6. The two strains were then mixed at a 1:1 cell ratio. The mixed culture was used to inoculate *E. scolopes* hatchlings, achieving a total concentration of ~ 103 CFU/ml. At 16 hpi, each individual squid was rinsed and relocated to a vial containing 5 ml FSOW. The water in the vial was exchanged every 24 h. Squid colonization was monitored by measuring the luminescence of the animals once a day using a TD 20/20 luminometer (Turner Designs, Sunnyvale, CA). At 24-h intervals a portion of the colonized squid were killed and stored at –80°C. These squid were subsequently homogenized, and dilutions plated on LBS agar. The relative competitive index (RCI) of the strains was determined as previously described (Bennett *et al.*, 2020). Briefly, the RCI is defined as: $\log_{10}$[(mutant CFU per ml in organ/wild-type CFU per ml in organ)/(mutant CFU per ml in the inoculum/wild-type CFU per ml in the inoculum)].

Light microscopy and fluorescence imaging

Unless stated otherwise, imaging for all experiments was conducted using a Zeiss LSM 980 confocal microscope with a Plan Apochromat 1.4 NA 100X oil objective. Stock solutions of two PG labels: (i) fluorescent HADA and (ii) the dipeptide probe EDADA were prepared at a concentration of 100 mM in DMSO, and stored at -20°C. HADA and EDADA short-pulse labeling and pulse-chase timelapse were

performed as previously described (Liechti *et al.*, 2016; Hsu *et al.*, 2017; Radkov *et al.*, 2018; Hsu *et al.*, 2019). For label-incorporation experiments, stocks were diluted to a final concentration of 1 mM in 0.3 ml of bacterial cultures. For short-pulse labeling, cultures were incubated at 28°C for 5 min. Cells were fixed by adding 0.7 ml of ice-cold ethanol, and incubated on ice for 1 h. Post-fixation, cells were pelleted by centrifugation (10,000 g for 1 min), washed with 1X marine phosphate-buffered saline (mPBS; Essock-Burns *et al.*, 2023), and resuspended in 1X mPBS for imaging. For fluorescence imaging, samples were prepared on 24 × 50 mm coverslips using a 1.5% SeaKem LE Agarose pad in mPBS. The coverslip–pad assemblies were positioned on a custom slide holder with the pad facing up for inverted microscopy. Click chemistry utilized a clickable Alexa Fluor 488 and a Click-iT Cell Reaction Buffer kit (Invitrogen), followed by three washes in 1X mPBS before imaging. Pulse-chase experiments involved incubating bacterial cells with 1 mM HADA for two doubling times, washing, and imaging on agarose pads. Pseudo pulse-chase experiments were conducted after incubating the bacterial cultures with 1 mM HADA for two doubling times, washing and incubating in fresh LBS medium. Cultures were then sampled every 8 min, fixed with 70% ethanol, and imaging on agarose pads.

To conduct short-pulse labeling of symbionts in juvenile *E. scolopes* squid, individual animals maintained for different time intervals ranging from 38 to 50 h posthatching were placed in FSOW containing 1 mM HADA for 1 h, fixed in 4% paraformaldehyde (PFA) in 1 × mPBS for 24 h. Tissue dissection, followed by TO-PRO-3 staining, was performed to label the nuclei of the crypt tissue. Samples were mounted in Vectashield (Vector Laboratories, Burlingame, CA) for imaging with a Zeiss LSM 800 confocal microscope.

Image analyses

Cell-length data were obtained using FIJI (Fiji Is Just ImageJ). Briefly, phase micrographs were imported into FIJI and cell lengths were manually traced using the "Freehand line" tool. Cell lengths were determined from the manual trace using the "Measure" function, calibrated to the μm/pixel scale of the original micrograph. The average fluorescence intensity per cell and cell area were measured using MicrobeJ (Ducret *et al.*, 2016).

Fluorescence intensity is defined as the average gray value measured on the channel used to detect the particle. All statistical analyses and data visualization were prepared using Prism (Field, 2002). To generate demographs and kymographs, fluorescence-intensity profiles were measured with ImageJ 1.47v (http://imagej.nih.gov/ij). The data were then processed in R version 3.5.0 using the Cell Profiles script (http://github.com/ta-cameron/Cell-Profiles) for demographs, as previously described (Cameron *et al.*, 2014). Additionally, MicrobeJ was also applied to generate the kymographs (Ducret *et al.*, 2016).

Marker frequency analysis (MFA)

Whole-genome sequencing reads were mapped to the *V. fischeri* ES114 chromosomes I and II (NCBI GenBank CP000020.2 and CP000021.2, respectively) with Bowtie2 v2.4.5 (Langmead and Salzberg, 2012), separately, with default parameters. SAMtools v1.16.1 (Danecek *et al.*, 2021) and BEDtools v2.40.0 (Quinlan and Hall, 2010) were used to report the read depth per base for each chromosome, and for every sample. Sliding-window averages of single-base coverages were obtained with the function "rollapply" from the R package "zoo" v1.8.11 (Zeileis and Grothendieck, 2005), with 1 kb-wide windows spaced 1 kb apart. Windows were removed if they had an internal SD that exceeded the median SD of all windows plus/minus 3X the difference between the median and the third quartile of all windows in the chromosome. For subsequent analyses and visualization, chromosome positions were adjusted (see Supplemental Material for details). After plotting the scatter of the window averages over chromosome position, two regression lines were calculated so that their y-intercepts were equal, while their x-intercepts and slopes had equal absolute values but opposite signs. The copy number at any given window on a chromosome was estimated by dividing the average coverage at that window by the ter coverage of the chromosome. Ori and ter copy numbers were estimated this way using averages of the windows that included positions 0 and 1, respectively.

mRNA visualization by HCR

Hybridization chain-reaction fluorescence in situ hybridization (HCR) (https://doi.org/10.1038/nbt.1692) was performed on light organs dissected from squid colonized with either wild-type or Δ*ldtA V. fischeri* strains carrying a *gfp*-labeled plasmid as previously described (6). Briefly, juvenile squid were fixed in 4% PFA in mPBS at either 4 h after dawn or 4 h after dusk. HCR probes [version 3.0 chemistry (https://doi.org/10.1242/dev.165753)] were designed to *V. fischeri ldtA* mRNA, and provided by Molecular Technologies (www.moleculartechnologies.org). 20 probes targeting *ldtA* mRNA were amplified with Alexa Fluor 488-labeled hairpins. Light organs were counterstained overnight with TO-PRO-3 and mounted on slides with Vectashield (Vector Laboratories, Burlingame, CA). Imaging was performed on an inverted Zeiss LSM 800 laser scanning confocal microscope at the Caltech Biological Imaging Facility. The resulting images were analyzed using FIJI (ImageJ).

HCR was also conducted on *V. fischeri* wild-type and Δ*ldtA* strains carrying an rfp-labeled plasmid, obtained from bacterial cell cultures during both the exponential phase (OD 0.5) and stationary phase (OD 4.0). In brief, the *V. fischeri* cells were fixed in a solution of 4% PFA in mPBS, and treated with 1 mg lysozyme per ml in 10 mM Tris-HCl (pH 7.6), with shaking at 37°C for 1 h. 20 probes targeting *ldtA* mRNA were amplified using Alexa Fluor 488-labeled hairpins. The sample was then resuspended in 5 × SSC-Tween (1 × SSC consisting of 0.15 M NaCl and 0.015 M sodium citrate, 0.1% Tween 20). Subsequently, 1 μl of labeled cells was spotted onto a coverslip and covered with a pad composed of 1% agarose in mPBS.

ACKNOWLEDGMENTS

The authors would like to thank the Ruby and McFall-Ngai laboratories for helpful discussions, and especially Joani Viliunas for extracting symbiont RNA, Vera Beilinson for analyzing the NanoString data, and Vanya Tepavcevic and Eve Otjacques for proofreading. We would also like to thank the Caltech Biological Imaging Center, where we performed much of the microscopy imaging. This work was supported by National Institutes of Health grants R37 AI50661 (to M.M.-N. and E.R.), and R01 OD11024 and R01 GM135254 (to E.R. and M.M.-N.), as well as R35 GM148385 (to M.J.M.).

REFERENCES

Adin DM, Engle JT, Goldman WE, McFall-Ngai MJ, Stabb EV (2009). Mutations in *ampG* and lytic transglycosylase genes affect the net release of peptidoglycan monomers from *Vibrio fischeri*. J Bacteriol 191, 2012–2022.

Alvarez L, Hernandez SB, Cava F (2021). Cell wall biology of *Vibrio cholerae*. Annu Rev Microbiol 75, 151–174.

Aschtgen MS, Wetzel K, Goldman W, McFall-Ngai M, Ruby E (2016). *Vibrio fischeri*-derived outer membrane vesicles trigger host development. Cellul Microbiol 18, 488–499.

Azimi S, Klementiev AD, Whiteley M, Diggle SP (2020). Bacterial quorum sensing during infection. Annu Rev Microbiol 74, 201–219.

Bennett BD, Essock-Burns T, Ruby EG (2020). HbtR, a heterofunctional homolog of the virulence regulator TcpP, facilitates the transition between symbiotic and planktonic lifestyles in *Vibrio fischeri*. mBio 11, e01624-20.
Bergkessel M, Basta DW, Newman DK (2016). The physiology of growth arrest: uniting molecular and environmental microbiology. Nat Rev Microbiol 14, 549–562.
Bergkessel M, Delavaine L (2021). Diversity in starvation survival strategies and outcomes among heterotrophic proteobacteria. Microb Physiol 31, 146–162.
Bertani G (1951). Studies on lysogenesis. I. The mode of phage liberation by lysogenic *Escherichia coli*. J Bacteriol 62, 293–300.
Boamah D, Gilmore MC, Bourget S, Ghosh A, Hossain MJ, Vogel JP, Cava F, O'Connor TJ (2023). Peptidoglycan deacetylation controls type IV secretion and the intracellular survival of the bacterial pathogen *Legionella pneumophila*. Proc Natl Acad Sci USA 120, e2119658120.
Boettcher K, Ruby E (1990). Depressed light emission by symbiotic *Vibrio fischeri* of the sepiolid squid *Euprymna scolopes*. J Bacteriol 172, 3701–3706.
Boettcher K, Ruby E, McFall-Ngai M (1996). Bioluminescence in the symbiotic squid *Euprymna scolopes* is controlled by a daily biological rhythm. J Comp Physiol 179, 65–73.
Bosco-Drayon V, Poidevin M, Boneca IG, Narbonne-Reveau K, Royet J, Charroux B (2012). Peptidoglycan sensing by the receptor PGRP-LE in the *Drosophila* gut induces immune responses to infectious bacteria and tolerance to microbiota. Cell Host Microbe 12, 153–165.
Brown CT, Olm MR, Thomas BC, Banfield JF (2016). Measurement of bacterial replication rates in microbial communities. Nat Biotechnol 34, 1256–1263.
Cameron TA, Anderson-Furgeson J, Zupan JR, Zik JJ, Zambryski PC (2014). Peptidoglycan synthesis machinery in *Agrobacterium tumefaciens* during unipolar growth and cell division. mBio 5, e01219-14.
Castanheira S, Cestero JJ, Rico-Pérez G, García P, Cava F, Ayala JA, Pucciarelli MG, García-del Portillo F (2017). A specialized peptidoglycan synthase promotes *Salmonella* cell division inside host cells. mBio 8, e01685-17.
Daas MC, de Roos NM (2021). Intermittent fasting contributes to aligned circadian rhythms through interactions with the gut microbiome. Benef Microbes 12, 147–161.
Danecek P, Bonfield JK, Liddle J, Marshall J, Ohan V, Pollard MO, Whitwham A, Keane T, McCarthy SA, Davies RM (2021). Twelve years of SAMtools and BCFtools. Gigascience 10, giab008.
Ducret A, Quardokus EM, Brun YV (2016). MicrobeJ, a tool for high throughput bacterial cell detection and quantitative analysis. Nat Microbiol 1, 16077.
Dunn AK, Millikan DS, Adin DM, Bose JL, Stabb EV (2006). New rfp- and pES213-derived tools for analyzing symbiotic *Vibrio fischeri* reveal patterns of infection and lux expression in situ. Appl Environ Microbiol 72, 802–810.
Egan AJ, Errington J, Vollmer W (2020). Regulation of peptidoglycan synthesis and remodelling. Nat Rev Microbiol 18, 446–460.
Essock-Burns T, Bongrand C, Goldman WE, Ruby EG, McFall-Ngai MJ (2020). Interactions of symbiotic partners drive the development of a complex biogeography in the squid-vibrio symbiosis. mBio 11, e00853-20
Essock-Burns T, Lawhorn S, Wu L, McClosky S, Moriano-Gutierrez S, Ruby EG, McFall-Ngai MJ (2023). Maturation state of colonization sites promotes symbiotic resiliency in the *Euprymna scolopes-Vibrio fischeri* partnership. Microbiome 11, 68.
Field AJ (2002). Computer performance evaluation: modelling techniques and tools. 12th International Conference, TOOLS 2002 London, UK, April 14-17, 2002 Proceedings, Springer Science & Business Media.
Frazier K, Leone VA (2022). Host-microbe circadian dynamics: Finding a rhythm and hitting a groove in scientific inquiry. Cell Host Microbe 30, 458–462.
Galli E, Paly E, Barre F-X (2017). Late assembly of the *Vibrio cholerae* cell division machinery postpones septation to the last 10% of the cell cycle. Sci Rep 7, 44505.
García-del Portillo F (2020). Building peptidoglycan inside eukaryotic cells: A view from symbiotic and pathogenic bacteria. Mol Microbiol 113, 613–626.
Garde S, Chodisetti PK, Reddy M (2021). Peptidoglycan: structure, synthesis, and regulation. EcoSal Plus 9, https://doi.org/10.1128/ecosalplus.ESP-0010-2020.
Goh YJ, Barrangou R, Klaenhammer TR (2021). *In vivo* transcriptome of *Lactobacillus acidophilus* and colonization impact on murine host intestinal gene expression. mBio 12, e03399-20.
Gokulan K, Varughese KI (2019). Drug resistance in *Mycobacterium tuberculosis* and targeting the L,D-transpeptidase enzyme. Drug Devel Res 80, 11–18.
Graf J, Dunlap PV, Ruby EG (1994). Effect of transposon-induced motility mutations on colonization of the host light organ by *Vibrio fischeri*. J Bacteriol 176, 6986–6991.
Graf J, Ruby EG (1998). Host-derived amino acids support the proliferation of symbiotic bacteria. Proc Natl Acad Sci USA 95, 1818–1822.
Guckes KR, Cecere AG, Wasilko NP, Williams AL, Bultman KM, Mandel MJ, Miyashiro T (2019). Incompatibility of *Vibrio fischeri* strains during symbiosis establishment depends on two functionally redundant *hcp* genes. J Bacteriol 201, e00221-19.
Hernández SB, Castanheira S, Pucciarelli MG, Cestero JJ, Rico-Pérez G, Paradela A, Ayala JA, Velázquez S, San-Félix A, Cava F (2022). Peptidoglycan editing in non-proliferating intracellular *Salmonella* as source of interference with immune signaling. PLoS pathogens 18, e1010241.
Higgins SA, Mann M, Heck M (2022). Direct DNA sequencing of '*Candidatus* Liberibacter asiaticus' from *Diaphorina citri*, the Asian citrus psyllid, and its implications for citrus greening disease management. bioRxiv, https://doi.org/10.1101/2022.01.28.478250.
Hsu Y-P, Hall E, Booher G, Murphy B, Radkov AD, Yablonowski J, Mulcahey C, Alvarez L, Cava F, Brun YV (2019). Fluorogenic D-amino acids enable real-time monitoring of peptidoglycan biosynthesis and high-throughput transpeptidation assays. Nat Chem 11, 335–341.
Hsu YP, Rittichier J, Kuru E, Yablonowski J, Pasciak E, Tekkam S, Hall E, Murphy B, Lee TK, Garner EC, *et al.* (2017). Full color palette of fluorescent d-amino acids for in situ labeling of bacterial cell walls. Chem Sci 8, 6313–6321.
Khanna K, Lopez-Garrido J, Pogliano K (2020). Shaping an endospore: Architectural transformations during *Bacillus subtilis* sporulation. Annu Rev Microbiol 74, 361–386.
Koch EJ, Miyashiro T, McFall-Ngai MJ, Ruby EG (2014). Features governing symbiont persistence in the squid–vibrio association. Mol Ecol 23, 1624–1634.
Koropatnick TA, Engle JT, Apicella MA, Stabb EV, Goldman WE, McFall-Ngai MJ (2004). Microbial factor-mediated development in a host-bacterial mutualism. Science 306, 1186–1188.
Kuru E, Hughes HV, Brown PJ, Hall E, Tekkam S, Cava F, de Pedro MA, Brun YV, VanNieuwenhze MS (2012). In situ probing of newly synthesized peptidoglycan in live bacteria with fluorescent D-amino acids. Angew Chem Int Ed Engl 124, 12687–12691.
Langmead B, Salzberg SL (2012). Fast gapped-read alignment with Bowtie 2. Nat Meth 9, 357–359.
Levy A, Conway JM, Dangl JL, Woyke T (2018). Elucidating bacterial gene functions in the plant microbiome. Cell Host Microbe 24, 475–485.
Liechti G, Kuru E, Hall E, Kalinda A, Brun Y, VanNieuwenhze M, Maurelli A (2014). A new metabolic cell-wall labelling method reveals peptidoglycan in *Chlamydia trachomatis*. Nature 506, 507–510.
Liechti G, Kuru E, Packiam M, Hsu YP, Tekkam S, Hall E, Rittichier JT, VanNieuwenhze M, Brun YV, Maurelli AT (2016). Pathogenic chlamydia lack a classical sacculus but synthesize a narrow, mid-cell peptidoglycan ring, regulated by MreB, for cell division. PLoS Pathog 12, e1005590.
Lupp C, Ruby EG (2005). *Vibrio fischeri* uses two quorum-sensing systems for the regulation of early and late colonization factors. J Bacteriol 187, 3620–3629.
Lynch JB, Bennett BD, Merrill BD, Ruby EG, Hryckowian AJ (2022). Independent host-and bacterium-based determinants protect a model symbiosis from phage predation. Cell Rep 38, 110376.
Mandel MJ, Schaefer AL, Brennan CA, Heath-Heckman EA, DeLoney-Marino CR, McFall-Ngai MJ, Ruby EG (2012). Squid-derived chitin oligosaccharides are a chemotactic signal during colonization by *Vibrio fischeri*. Appl Environ Microbiol 78, 4620–4626.
McFall-Ngai MJ, Ruby EG (1991). Symbiont recognition and subsequent morphogenesis as early events in an animal-bacterial mutualism. Science 254, 1491–1494.
Meyer KM, Deines P, Wei Z, Busby PE, Lindow SE, Bohannan BJ (2022). The role of dispersal and transmission in structuring microbial communities. Front Microbiol 13, 1054498.
Montgomery MK, McFall-Ngai M (1993). Embryonic development of the light organ of the sepiolid squid *Euprymna scolopes* Berry. Biol Bull 184, 296–308.
Morè N, Martorana AM, Biboy J, Otten C, Winkle M, Serrano CKG, Montón Silva A, Atkinson L, Yau H, Breukink E (2019). Peptidoglycan remodeling enables *Escherichia coli* to survive severe outer membrane assembly defect. mBio 10. e02729-18.

Moriano-Gutierrez S, Koch EJ, Bussan H, Romano K, Belcaid M, Rey FE, Ruby EG, McFall-Ngai MJ (2019). Critical symbiont signals drive both local and systemic changes in diel and developmental host gene expression. Proc Natl Acad Sci USA 116, 7990–7999.
Nyholm SV, McFall-Ngai MJ (2021). A lasting symbiosis: how the Hawaiian bobtail squid finds and keeps its bioluminescent bacterial partner. Nat Rev Microbiol 19, 666–679.
Papadopoulos AO, Ealand C, Gordhan BG, VanNieuwenhze M, Kana BD (2021). Characterisation of a putative M23-domain containing protein in *Mycobacterium tuberculosis*. PLoS One 16, e0259181.
Peters K, Kannan S, Rao VA, Biboy J, Vollmer D, Erickson SW, Lewis RJ, Young KD, Vollmer W (2016). The redundancy of peptidoglycan carboxypeptidases ensures robust cell shape maintenance in *Escherichia coli*. mBio 7, e00819-16.
Pisabarro AG, de Pedro MA, Vázquez D (1985). Structural modifications in the peptidoglycan of *Escherichia coli* associated with changes in the state of growth of the culture. J Bacteriol 161, 238–242.
Quinlan AR, Hall IM (2010). BEDTools: a flexible suite of utilities for comparing genomic features. Bioinformatics 26, 841–842.
Radkov AD, Hsu YP, Booher G, VanNieuwenhze MS (2018). Imaging bacterial cell wall biosynthesis. Annu Rev Biochem 87, 991–1014.
Reed P, Atilano ML, Alves R, Hoiczyk E, Sher X, Reichmann NT, Pereira PM, Roemer T, Filipe SR, Pereira-Leal JB (2015). *Staphylococcus aureus* survives with a minimal peptidoglycan synthesis machine but sacrifices virulence and antibiotic resistance. PloS Path 11, e1004891.
Roller BRK, Hellerschmied C, Wu Y, Miettinen TP, Gomez AL, Manalis SR, Polz MF (2023). Single-cell mass distributions reveal simple rules for achieving steady-state growth. mBio 14, e01585–01523.
Ruby E, Asato L (1993). Growth and flagellation of *Vibrio fischeri* during initiation of the sepiolid squid light organ symbiosis. Arch Microbiol 159, 160–167.
Sauvage E, Kerff F, Terrak M, Ayala JA, Charlier P (2008). The penicillin-binding proteins: structure and role in peptidoglycan biosynthesis. FEMS Microbiol Rev 32, 234–258.
Schwartzman JA, Ruby EG (2016). Stress as a normal cue in the symbiotic environment. Trends Microbiol 24, 414–424.
Sezonov G, Joseleau-Petit D, d'Ari R (2007). *Escherichia coli* physiology in Luria-Bertani broth. J Bacteriol 189, 8746–8749.
Shaku M, Ealand C, Matlhabe O, Lala R, Kana BD (2020). Peptidoglycan biosynthesis and remodeling revisited. Adv Appl Microbiol 112, 67–103.
Silva AR, Sousa C, Exner D, Schwaiger R, Alves MM, Petrovykh DY, Pereira L (2021). pH-induced modulation of *Vibrio fischeri* population life cycle. Chemosensors 9, 283.
Skovgaard O, Bak M, Lobner-Olesen A, Tommerup N (2011). Genome-wide detection of chromosomal rearrangements, indels, and mutations in circular chromosomes by short read sequencing. Genome Res 21, 1388–1393.
Squeglia F, Ruggiero A, Berisio R (2018). Chemistry of peptidoglycan in *Mycobacterium tuberculosis* life cycle: an off-the-wall balance of synthesis and degradation. Chemistry 24, 2533–2546.
Stapels DAC, Hill PWS, Westermann AJ, Fisher RA, Thurston TL, Saliba AE, Blommestein I, Vogel J, Helaine S (2018). *Salmonella* persisters undermine host immune defenses during antibiotic treatment. Science 362, 1156–1160.
Stewart CJ, Ajami NJ, O'Brien JL, Hutchinson DS, Smith DP, Wong MC, Ross MC, Lloyd RE, Doddapaneni H, Metcalf GA (2018). Temporal development of the gut microbiome in early childhood from the TEDDY study. Nature 562, 583–588.
Stoudenmire JL, Essock-Burns T, Weathers EN, Solaimanpour S, Mrazek J, Stabb EV (2018). An iterative, synthetic approach to engineer a high-performance PhoB-specific reporter. Appl Environ Microbiol 84, e00603-18.
Studer SV, Mandel MJ, Ruby EG (2008). AinS quorum sensing regulates the *Vibrio fischeri* acetate switch. J Bacteriol 190, 5915–5923.
Troll JV, Adin DM, Wier AM, Paquette N, Silverman N, Goldman WE, Stadermann FJ, Stabb EV, McFall-Ngai MJ (2009). Peptidoglycan induces loss of a nuclear peptidoglycan recognition protein during host tissue development in a beneficial animal-bacterial symbiosis. Cell Microbiol 11, 1114–1127.
Troll JV, Bent EH, Pacquette N, Wier AM, Goldman WE, Silverman N, McFall-Ngai MJ (2010). Taming the symbiont for coexistence: a host PGRP neutralizes a bacterial symbiont toxin. Environ Microbiol 12, 2190–2203.
Typas A, Banzhaf M, Gross CA, Vollmer W (2012). From the regulation of peptidoglycan synthesis to bacterial growth and morphology. Nat Rev Microbiol 10, 123–136.
Val M-E, Marbouty M, de Lemos Martins F, Kennedy SP, Kemble H, Bland MJ, Possoz C, Koszul R, Skovgaard O, Mazel D (2016). A checkpoint control orchestrates the replication of the two chromosomes of *Vibrio cholerae*. Sci Adv 2, e1501914.
Visick KL, Foster J, Doino J, McFall-Ngai M, Ruby EG (2000). *Vibrio fischeri* lux genes play an important role in colonization and development of the host light organ. J Bacteriol 182, 4578–4586.
Visick KL, Stabb EV, Ruby EG (2021). A lasting symbiosis: How *Vibrio fischeri* finds a squid partner and persists within its natural host. Nat Rev Microbiol 19, 654–665.
Vollmer W, Bertsche U (2008). Murein (peptidoglycan) structure, architecture and biosynthesis in *Escherichia coli*. Biochim Biophys Acta Biomembr 1778, 1714–1734.
Vollmer W, Blanot D, De Pedro MA (2008). Peptidoglycan structure and architecture. FEMS Microbiol Rev 32, 149–167.
Wheatley RM, Ford BL, Li L, Aroney STN, Knights HE, Ledermann R, East AK, Ramachandran VK, Poole PS (2020). Lifestyle adaptations of *Rhizobium* from rhizosphere to symbiosis. Proc Natl Acad Sci USA 117, 23823–23834.
Yin L, Ma H, Nakayasu ES, Payne SH, Morris DR, Harwood CS (2019). Bacterial longevity requires protein synthesis and a stringent response. mBio 10, e02189-19.
Zeileis A, Grothendieck G (2005). zoo: S3 infrastructure for regular and irregular time series. arXiv, https://doi.org/10.48550/arXiv.math/0505527.